CrossMark

ORIGINAL PAPER

Mixed ionic and electronic conductivity study of charge transfer complexes of some substituted pyridines with iodine monochloride (ICl) by AC impedance spectroscopy

Uttam Mohan [1,2] · Pallavi Gogoi [3] · S. K. Baruah [2]

Abstract Mixed ionic and electronic conductivity of three solid charge transfer (CT) complexes of pyridine, 4-methylpyridine (γ-picoline) and 3,5-dimethylpyridine (3,5-lutidine) with ICl (iodine monochloride) are reported. Electrical parameters of the prepared complexes in the pellet form are evaluated at various temperatures and at wide frequency range by employing AC complex impedance spectroscopic technique. Suitable equivalent circuits for the Nyquist plots, which provide the most realistic model of the electrical properties of the CT complexes, have been suggested. Both transport number measurements and impedance spectra reveal that the conduction in γ-picoline-ICl complex is mainly due to ions, in 3,5-dimethylpyridine-ICl complex, it is due to both ions and electrons and in pyridine-ICl complex, it is predominantly due to electrons. The a.c. conductivity measurements of the CT complexes have been carried out in the frequency range of 10–10^5 Hz within the temperature range of 303–353 K. The variation of a.c. conductivity with frequency follows the Jonscher's universal power law. The temperature dependence of electrical conductivity suggests the semiconducting behaviour of the materials.

✉ Uttam Mohan
uttamohan@rediffmail.com

1   D. H.S.K. College, Dibrugarh, Assam, India

2   Department of Chemistry, Dibrugarh University, Dibrugarh, Assam, India

3   Department of Chemistry, Tinsukia College, Tinsukia, Assam, India

Introduction

The intermolecular interaction between electron donor D and electron acceptor A leads to the formation of a new molecular assembly, DA, called charge transfer (CT) complex, first introduced by Mulliken [1, 2]. Organic CT complexes and salts have extensively been investigated in various areas of chemistry and material sciences both from the theoretical and experimental aspects as they exhibit diverse kind of interesting physical properties and functionalities related to optical, magnetic, electrical (super) conductivity and dielectric properties [3, 4]. Since the discovery of the first metallic type CT complex TTF-TCNQ in 1973 [5], attention to organic CT complexes has been focussed for several decades, aimed mainly at the discovery of materials with good electrical conductivity or even room temperature superconductivity [6]. Later on, attention has been turned to technologically relevant properties of CT complexes due to their potential in the improvement of electronic and optoelectronic devices [7].

The solid organic CT complexes are one of the most important subclasses of organic semiconductors [8, 9] which often exhibit similar conduction mechanism to inorganic semiconductors where hole and electron conduction layers are typical carriers separated by a band gap. CT complexes exhibiting mixed ionic-electronic conduction have also been reported [10–13].

Although, the electrical conductivity of charge transfer complexes of pyridine analogue with halogens and interhalogens has been reported in literatures [14–16]; however, the detailed studies of frequency dependence a.c. conductivity and complex impedance spectroscopy of these complexes

are lacking. In this paper, the electrical properties of the CT complexes obtained by the interactions of three n-donors namely pyridine, 4-methylpyridine and 3,5-dimethylpyridine with iodine monochloride (ICl) as σ-acceptor are reported.

Despite the fact that the electrical conduction property of a donor-acceptor complex depends upon many factors, to manifest high conductivity, the mixed valence (or partial CT state) electronic structure and specific molecular packing architecture (segregated stacking and mixed stacking) within the molecular assembly are the most essential criteria [17]. The degree of charge transfer, δ from donor (D) to acceptor (A), in the complex $(D^{+\delta}A^{-\delta})$ is primarily governed by the ionization potential (I_p) of D and electron affinity (E_a) of A. A neutral CT complex with $\delta = 0$ is obtained if $E_a > I_p$, whereas the completely ionic state corresponds to $\delta = 1, 2.....$ when $E_a < I_p$. Both neutral and completely ionic CT complexes are insulators with few exceptions [18, 19]. It is reported [7, 20] that mixed valence CT complexes within the window $0.50 < \delta < 0.74$ with segregated stacks of the D and A components generally exhibit metallic electrical conduction; otherwise, alternating stack CT complexes are either semiconductors or insulators.

For the study of microstructural and electrical properties of many electronic materials, the AC impedance spectroscopy has long been used as a non-destructive experimental technique [21]. In this technique, a sinusoidal perturbation is applied on the test system and the AC response is analysed. The ratio of the voltage response to the current perturbation is the impedance which is calculated as a function of the frequency of the perturbation. The interpretations of the impedance spectra $(-Z''_{im}$ vs $Z'_{real})$ are aided by analogy to physically plausible equivalent circuits involving simple components such as capacitors and resistors connected in many modes. From this analysis, a meaningful insight into the material behaviour can be obtained. The analysed values of the electrical parameters (conductivity, dielectric constant, loss, capacitance, etc.) give explicit results when compared with those measured at arbitrarily selected fixed frequencies. This powerful technique is useful for the measurement of real and imaginary part of impedances for a wide range of frequency, determination of relaxation frequency and separation of grain, grain boundary and grain-electrode effects [22, 23].

Experimental

Materials

Pyridine (from Ranbaxy Lab. Ltd.), 4-methylpyridine (from Sigma Aldrich), 3,5-dimethylpyridine (from Sigma Aldrich) and ICl (from Ranbaxy fine chemical Ltd.) were used without further purification. Hexane (Merck) was used after distillation as a solvent.

Synthesis and characterization of complexes

The solid CT complexes of the pyridine analogue with ICl were prepared by stirring equimolar quantities of the donor with ICl in hexane, which resulted in precipitation of the complex as light yellow solid. The separated solids were filtered and washed several times with minimum amount of hexane and these are dried under vacuum over anhydrous calcium chloride. The resultant complexes were characterised by routine techniques like elemental analysis, UV-Vis, FTIR, ^{1}H-NMR spectroscopy and powder XRD.

The elemental analysis of the carbon, hydrogen and nitrogen content was performed by using Perkin Elmer CHN 2400 Series II analyzer. The total halogen contents were estimated by a simple gravimetric method with AgNO$_3$ solution.

The electronic absorption spectra of the donors, acceptor and the resulting complexes in hexane were recorded over a wavelength range of 200–900 nm using Shimadzu U-3900 spectrophotometer. The diffuse reflectance spectra of the solids were recorded with a JASCO V-750 UV Visible spectrophotometer in the region 200–900 nm.

The FT-IR spectra were recorded on a Shimadzu FT-IR spectrophotometer (IRPrestige-21) within the range of 4000–250 cm^{-1}.

The ^{1}H-NMR spectra were recorded in CDCl$_3$ solvent. Powder XRD analysis was carried out at room temperature by using Cu radiation ($\lambda = 1.5405$ Å) in the range $2° \leq 2\theta \leq 70°$ at a scanning rate of 1°/min and step height of 0.05°.

Electrical properties

The solid complexes were pelletized into discs of 13 mm diameter by using a hydraulic press (Spectralab) at a pressure of 9 Kbar. The thicknesses (0.5 to 1.5 mm) were measured with a screw gauge. Uniform graphite layer was applied on the opposite faces of the pellets and was sandwiched between two thin sheets of copper electrodes with even surface. Before recording the data, each sample was sintered at 50 °C for 30 min to ascertain the interface contact between the electrodes and the sample. The electrical properties were measured by complex impedance method using LCR HiTester (HIOKI 3522) frequency response analyser in the frequency range from 10 Hz to 100 kHz. AC conductance (G), impedance (Z) and phase angle (θ) were measured as a function of frequency at different temperatures. The sample cell was kept for 30 min at each measuring temperature in order to reach its thermal equilibrium. The impedance spectra were modelled as an 'equivalent circuit' by using complex non-linear least squares fitting of both real and imaginary part of impedance. LEVM 3.0 software [24] has been used for fitting purpose. The best fitted equivalent circuit has been determined by observing the coherence between the experimental and the simulated data

in the complex impedance plots. D.C. conductance of the pellets was measured at various temperatures by using Keithley 2400 source meter. Electrical conductivity was calculated using the pellet dimensions and the measured resistance.

Determination of ionic transport number

The total ionic transport numbers, t_{ion}, were evaluated by the standard Wagner polarization technique [25]. The cell 'SS| CT complex |SS' was polarized by a step potential of about 1 V and the resulting current was monitored as a function of time [26, 27], where SS stands for stainless steel. The SS acted as blocking electrodes for the above cell. The t_{ion} values were evaluated from the polarization current curve by using the following equation:

$$t_{ion} = \frac{(i_i - i_f)}{i_i} \qquad (1)$$

where i_i and i_f are the initial and final steady state currents, respectively.

Results and discussion

Elemental analysis

Elemental analyses data (C, H, N and total halogen) of the complexes were given in Table 1. It is observed that the experimental values agree quite well with the calculated values for 1:1 complexes. The same stoichiometries in the solution state are confirmed by the linearity of the Benesi-Hildebrand plots (S1).

UV-Vis spectroscopy

In the electronic absorption spectra (S2) of the resulting complexes (in hexane), an additional absorption band at λ_{max} = 333.4, 316.8 and 322.4 nm for pyridine-ICl, 4-methylpyridine-ICl and 3,5-dimethylpyridine-ICl complexes, respectively, indicates the formation of CT complexes.

In the diffuse reflectance spectra of the solid complexes (Fig. 1), the bands at 256, 322 and 371 nm for pyridine-ICl, at 239, 262, 301 and 361 nm for 3,5-dimethylpyridine-ICl and at 253, 312 and 427 nm for 4-methylpyridine-ICl complexes
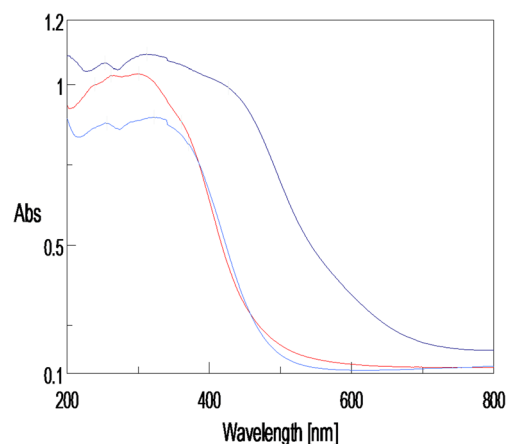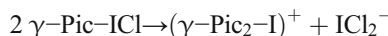

Fig. 1 Diffuse reflectance spectra of pyridine-ICl (*blue*), 3,5-dimethylpyridine-ICl (*red*) and 4-methylpyridine-ICl (*purple*) complexes

indicate the presence of ICl_2^- ion in the solid state [28]. The formation of ICl_2^- ion is attributed to the solid state transformation of the CT complexes (e.g. 4-methylpyridine-ICl) as follows:

$$2\,\gamma\text{-Pic-ICl} \rightarrow (\gamma\text{-Pic}_2\text{-I})^+ + ICl_2^-$$

The optical band gaps of the CT complexes were estimated from the optical absorption edge of the spectrum by using the Tauc relation [29]

$$A h\nu = (h\nu - E_g)^n \qquad (2)$$

where A is the absorbance, E_g is the optical band gap corresponding to a particular absorption of photon of energy $h\nu$ and n is ½ for allowed direct, 3/2 for forbidden direct, 2 for allowed indirect and 3 for forbidden indirect transitions in the material. It is observed that $(A h\nu)^{1/2}$ versus $h\nu$ plots are linear (Fig. 2) and the intercept on the energy axis on extrapolating; the linear portion of the curves to A = 0 gives the indirect band gap. The values of E_g are given in Table 2.

FTIR spectroscopy

Few selected IR frequencies of the donor on complex formation are affected in both intensities and wave number values (S3a–c). This could be interpreted on the basis of expected electronic environment change upon

Table 1 Elemental analysis data of the CT complexes

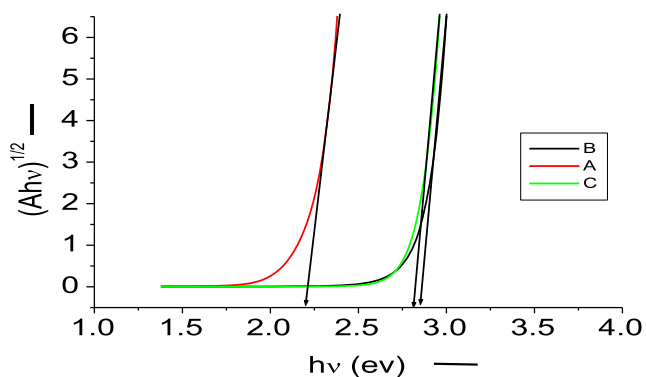| Complex	C, %		H, %		N, %		Halogens, %	
	Cal.	Found	Cal.	Found	Cal.	Found	Cal.	Found
Py-ICl	24.86	24.36	2.07	2.12	5.80	5.62	67.26	67.05
4-MePy-ICl	28.19	28.25	2.74	3.04	5.48	5.30	63.58	63.84
3,5-DiMePy-ICl	31.18	30.60	3.34	3.37	5.19	5.24	60.28	60.33

Fig. 2 (Ahν)$^{1/2}$ vs hν (photon energy) plot of **A** 4-methylpyridine-ICl (*red*), **B** 3,5-dimethylpyridine-ICl (*black*) and **C** pyridine-ICl (*green*) complexes

Table 2 Physical properties, optical band gap and ionic transport no. of the CT complexes

Complex	Colour	m.p. (K)	E_g (ev)	t_{ion}
Py-ICl	Light yellow	132	2.85	0.11
4-MePy-ICl	Yellow	113	2.21	0.95
3,5-DiMePy-ICl	Light yellow	170	2.78	0.58

complexation. The detailed vibrational assignments were reported in Table 3. These assignments were in accordance with earlier works [30, 31].

It is observed that the spectra of the CT complexes show all the principal features for free donors. Many modes on complex formation have been shifted to higher frequency in comparison to the free donor. Similar upward shifts were observed for metal coordinated pyridine [32] and metal coordinated pyridine analogues [33, 34]. It has been reported [35] that iodine monochloride (ICl) has an allowed fundamental absorption at 382 cm^{-1} in the gas phase and the I-Cl stretching frequency decreases on complex formation with strong donor like pyridine. The bands at 290 cm^{-1} for pyridine-ICl, 265 cm^{-1} for 4-methylpyridine-ICl and 273 cm^{-1} for 3,5-dimethylpyridine-ICl complexes have been assigned to I-Cl stretching in the complexes [36].

^{1}H-NMR spectra

The ^{1}H-NMR spectra of CT complexes (S4a-c) showed the δ values for ring and methyl group protons in the donor molecules are shifted towards lower field (Table 4). The smallest change was observed for α protons on comparing the chemical shifts of β, γ and methyl protons; it could be explained by the paramagnetic effect observed previously [37] in free donors. The observed down-field shift for all protons is attributed to the decrease of electron density on each ring carbon as a consequence of partial positive charge at the nitrogen atom on complex formation.

Table 3 FTIR frequencies (cm^{-1}) of the donors and their CT complexes

Pyridine	Py-ICl	4-MePy	4-MePy-ICl	3,5-DiMePy	3,5-DiMePy –ICl	Assignment
3074s	3093s	3066w	3139w	3020s	3049s	C–H stretching
3026s	3063s	2960w	3080m	2980s	3014s	C–H stretching
–	–	2922m	2968vw	2866m	2900m	C–H (−CH$_3$) stretching
1923w	1845w	–	1928m	1860vw	1865w	overtone of C–H vibration
–	–	–	1836w	1792vw	1805w	overtone of C–H vibration
1580s	1599s	1589s	1610vs	1585s	1593s	C=N stretching
1481m	1525s	1458s	–	1458m	1466vw	C=C stretching
1439s	1477m	–	1421s	1427s	1442s	C=C stretching
–	1323w	1375w	1373w	1381m	1384m	Antisym. and Sym. CH$_3$ deformation
1215s	1244m	–	–	1234w	1267w	
1145s	1192m	1226vw	1249m	1166s	1170m	The C–H in-plane bending vibrations
1066m	1157m	1157w	1201s	1141m	1141s	C–N stretching
1029m	1060s	1059w	1060s	1039s	1047m	C–C deformation
991m	1014w	1031w	1020s	858s	869s	C–H torsion
700m	742m	777s	810vs	713s	759s	γ (C–H)
690w	684w	–	707w	–	692m	δ ring
605m	634w	–	545s	–	536vw	
405m	424vw	–	486s	–	–	γ ring
–	374s	–	358w	–	362s	X-sensitive
–	290s	–	265s	–	273s	ν$_{I–Cl}$

v- very, s- strong, m- medium, w- weak

Table 4 ^{1}H Chemical shifts (δ ppm) of the CT complexes and the parent donors

Compound	Hα	Δα	Hβ	Δβ	Hγ	Δγ	–CH$_3$ β	–CH$_3$γ	Δ–CH$_3$
Pyridine	8.50	–	7.04	–	7.46	–	–	–	–
Pyridine-ICl	8.67	0.17	7.47	0.43	8.02	0.56	–	–	–
4-methylpyridine	8.50	–	7.16	–	–	–	–	2.41	–
4-methylpyridine-ICl	8.51	0.01	7.28	0.12	–	–	–	2.48	0.07
3,5-dimethylpyridine	8.25	–	–	–	7.27	–	2.23	–	–
3,5-dimethylpyridine-ICl	8.29	0.04	–	–	7.60	0.33	2.40	–	0.17

Powder XRD analysis

The room temperature X-ray diffraction pattern of pyridine-ICl complex (S5a) showed a good agreement with the single crystal data [38]. The good agreement between the observed (d_{obs}) and calculated (d_{cal}) inter-planar spacing (Table 5) confirmed that the prepared complex has a monoclinic structure, as reported earlier, with unit cell lattice parameters a = 4.274 Å, b = 12.319 Å, c = 14.094 Å, β = 94.99° and unit cell volume 739.3 Å^3.

For the lack of crystal structure data about 4-methylpyridine-ICl and 3,5-dimethylpyridine-ICl complexes, Powder-X software has been applied in order to index the diffraction pattern. It is found that the diffraction pattern of both the complexes are best fitted to a monoclinic unit cell with the estimated lattice parameters

a = 8.335 Å, b = 12.830 Å, c = 18.313 Å, β = 90.03° and V = 1958.3 Å^3 for 4-methylpyridine-ICl and for 3,5-dimethylpyridine-ICl complex are a = 6.636 Å, b = 18.935 Å, c = 8.789 Å, β = 97.06° and V = 1095.99 Å^3. The inter-planar spacing (d_{hkl}) values were calculated by using Eq. (3) for monoclinic system and a quite good agreement between the observed (d_{obs}) and calculated (d_{cal}) values (Table 5) confirmed the estimated unit cell parameters.

$$\frac{1}{d_{hkl}^2} = \frac{h^2}{a^2 Sin^2\beta} + \frac{k^2}{b^2} + \frac{l^2}{c^2 Sin^2\beta} - \frac{2hlCos\beta}{acSin^2\beta} \qquad (3)$$

The average grain size (D) of the samples was calculated from the most intense x-ray diffraction peak by using the classical Scherer [39] formula

Table 5 Comparison of d_{obs} and d_{cal} (Å) values of some reflections for the CT crystals at room temperature

Pyridine-ICl			4-methylpyridine-ICl			3,5-dimethylpyridine-ICl		
h k l	d_{obs} (Å)	d_{cal} (Å)	h k l	d_{obs} (Å)	d_{cal} (Å)	h k l	d_{obs} (Å)	d_{cal} (Å)
0 0 2	7.049	7.073	0 1 1	10.766	10.508	1 1 1	7.788	7.872
0 1 2	6.087	6.126	0 0 4	4.588	4.578	0 3 1	6.385	6.235
0 2 1	5.605	5.675	0 1 4	4.350	4.312	0 1 3	4.523	4.552
0 2 2	4.607	4.660	1 0 4	4.032	4.013	1 0 3	4.095	4.030
0 1 3	4.361	4.407	1 2 3	3.920	3.907	0 3 3	3.877	3.875
0 3 0	4.022	4.130	1 3 2	3.510	3.514	1 4 2	3.800	3.799
0 3 1	3.949	3.965	2 1 3	3.323	3.325	0 5 2	3.587	3.588
0 2 3	3.775	3.752	2 0 4	3.079	3.082	0 0 4	3.510	3.498
0 3 2	3.697	3.567	3 1 2	2.580	2.604	3 5 0	3.088	3.086
0 0 4	3.531	3.537	1 4 4	2.509	2.506	4 4 0	2.866	2.868
0 3 3	3.084	3.107	2 1 6	2.416	2.418	0 5 4	2.685	2.682
0 4 0	3.047	3.098	1 4 5	2.315	2.318	2 5 4	2.307	2.308
0 2 4	3.000	3.071	–	–	–	4 3 3	2.277	2.278
0 4 1	2.955	3.026	–	–	–	4 4 3	2.167	2.188
0 4 2	2.859	2.837	–	–	–	3 5 4	2.094	2.094
0 3 4	2.753	2.686	–	–	–	–	–	–
0 4 3	2.661	2.589	–	–	–	–	–	–
1 0 0	2.547	2.483	–	–	–	–	–	–
1 1 1	2.320	2.366	–	–	–	–	–	–
1 3 1	2.072	2.082	–	–	–	–	–	–
1 3 2	1.977	1.997	–	–	–	–	–	–

$$D = \frac{K\lambda}{\beta \cos\theta} \qquad (4)$$

where λ is the x-ray wavelength (for Cu-Kα radiation $\lambda = 1.5405$ Å), K is a constant (0.90 for Cu grid), θ is the Bragg diffraction angle (half the scattering angle) and β is the full width at half maximum (FWHM) in radians of the main peak. The average particle size for pyridine-ICl, 4-methylpyridine-ICl and 3,5-dimethylpyridine-ICl complexes was found to be 55, 45 and 61 nm, respectively.

Impedance studies

The Nyquist diagrams ($-Z$ vs Z') are shown in Fig. 3a–c for pyridine-ICl at 303, 313, 318, 323, 333, 343 and 353 K; for 4-methylpyridine-ICl at 303, 313, 318, 323, 328, 333 and 338 K and for 3,5-dimethylpyridine-ICl at 303, 318, 323, 333, 338 and 343 K. The spectra 3a and 3c relative to pyridine-ICl and 3,5-dimethylpyridine-ICl consist of a single semicircle whose radii decrease with the rise in temperature. The spectra 3b related to 4-methylpyridine-ICl are characterised by the appearance of depressed semicircles at higher frequencies with an inclined spike on the low frequency side. The inclined spike on the low frequency side of the semicircles in the spectrum of 4-methylpyridine-ICl is a characteristic of polarization phenomena at the electrode-material interface. Hence, conduction in 4-methylpyridine-ICl is ascribed mainly due to ions. The absence of inclined spike in the impedance spectrum of pyridine-ICl and tiny spike like portion in the low frequency side of the impedance spectrum of 3,5-dimethylpyridine-ICl attribute to either electronic or mixed ionic-electronic conduction [40].

Equivalent circuit fitting

The electrical behaviour of a system can be interpreted in terms of an equivalent circuit containing real electrical elements in various combinations. It should be worth mentioning that a particular electrical circuit can be customized in a variety of combinations of simple electrical elements but at a halt results the same overall a.c. response. Though, there is no unique equivalent circuit for a particular system; however, an equivalent circuit can be selected on the basis of the following criteria:

(i)   Keeping in mind as to what kind of impedances is probable to be present in the system in question and how they connected.
(ii) Whether the response of the proposed circuit is consistent to the experimental data.
(iii) Whether the simulated values of the circuit elements (R, C, etc.) are realistic and their variation with temperature is logical.

In general, an equivalent circuit used to describe the impedances of polycrystalline solid materials consists of three parallel RC elements connected in series corresponds to grain interior, grain boundary and electrode [41]. A single parallel RC element gives one semicircular arc passing through the origin in the Nyquist $-Z$ vs Z' plot and the low frequency intercept on the real Z' axis corresponds to the resistance R of the element. We expect three semicircular arcs corresponds to the grain (bulk), grain boundary and electrode contributions. In practice, all the semicircles may not be noticed. They may overlap, depress or distort due to the presence of (i) distribution in relaxation times and (ii) very small differences of the time constants of various relaxation processes, if any. The non-ideal nature of the experimental impedance spectrum enforced to fit the experimental data to evaluate the contributions of various circuit elements which otherwise cannot be worked out from the experimental spectrum. In this paper, LEVM 3.0 software [24] has been used for fitting purpose.

Pyridine-ICl complex Although the impedance spectrum (Fig. 3a) seems like a single semicircle at the first sight, the experimental data did not fit well to an equivalent circuit containing a single parallel RC element. The best fit is achieved by using an equivalent circuit comprising of three RC elements connected in series (Fig. 4a). Hence, in this complex grain, grain boundary and electrode contributions are responsible for total hindrance in the material. The values of all parameters of the equivalent circuit, after fitting at different temperatures, are given in Table 6. The validity of the proposed equivalent circuit is confirmed by the excellent coherence between the experimental and the simulated data in the complex impedance plots. The temperature variation of the R_i parameters (in terms of σ_i) obeys the Arrhenius law (Fig. 5).

4-methylpyridine-ICl complex The existence of low frequency straight line indicates the presence of double layer capacitance of electrode-material interface [42] and the semicircular portion corresponds to the parallel combination of resistance and capacitance. But the angle of inclination of the straight line and depressed semicircle indicate the presence of distributed microscopic properties of the material, which is called constant phase element (cpe). Hence, cpe has been introduced in place of ideal capacitive circuit element. The experimental complex impedance spectrum can be best fitted to the equivalent circuit given in Fig. 4b. The depressed semicircle corresponds to the parallel combination of bulk resistance and a constant phase element (cpe) in series with another cpe corresponds to the inclined spike due to interfacial polarization. The inclined spike (as observed in case of a real solid electrolyte) in the complex impedance plot indicates that 4-methylpyridine-ICl complex is mainly ionic. However, for an ideal solid electrolyte, one would expect a vertical straight line (instead of inclined one) on the low frequency side followed by a perfect semicircle (instead of depressed one) in the complex impedance plot.

Fig. 3 Nyquist plots of **a** pyridine-ICl, **b** 4-methylpyridine-ICl and **c** 3, 5-dimethylpyridine-ICl complex
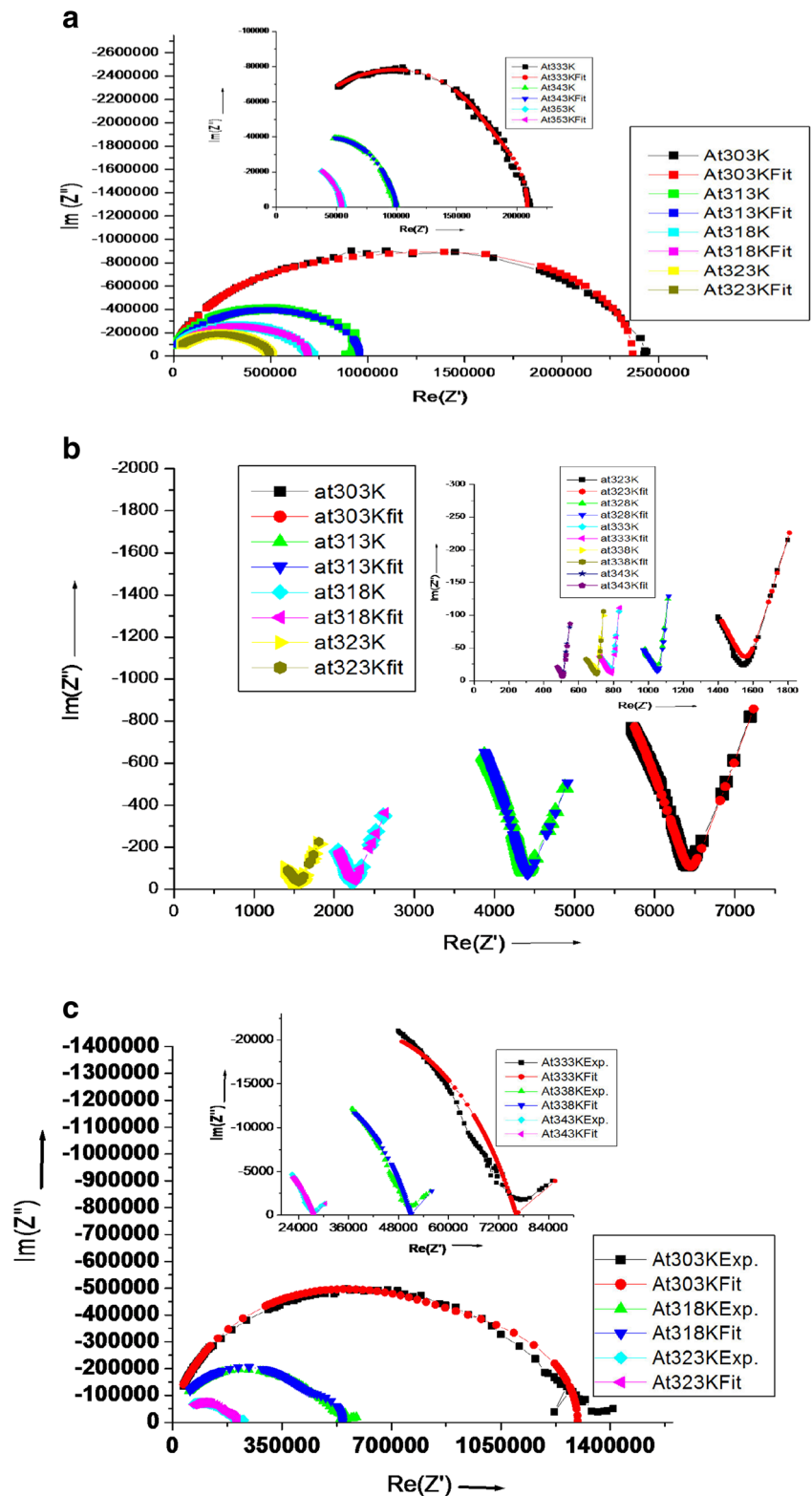
3,5-dimethylpyridine-ICl complex The impedance spectra at lower temperatures of this complex have been best fitted to an equivalent circuit comprising of three RC elements connected in series corresponding to grain, grain boundary and electrode interface. However, at 333 K and above, a spike at lower frequency region of the impedance spectra become prominent indicating different conduction mechanism at higher temperatures. Hence, similar equivalent circuit as that

Fig. 4 Equivalent circuit **a** –(RgCg)–(RgbCgb)–(RelCel)– and **b** –(Rcpe)–(cpe)–
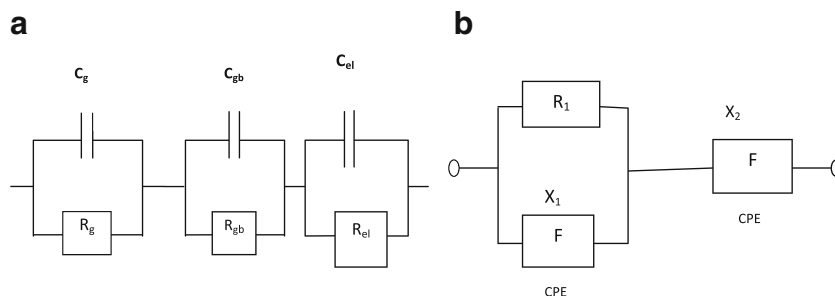
of 4-methylpyridine-ICl complex (i.e. 4b) is appropriate for the spectra at 333, 338 and 343 K. At higher temperatures, ionization of the complex transforms the material from mixed conductor to predominantly ionic conductor.

The total conductivity (σ_T) of the sample has been calculated using the total resistance and the dimensions of the pellet with the following equation:

$$\sigma_T = \frac{1}{R_T} \times \frac{t}{A} \tag{5}$$

where t is the thickness, A is the area of the pellet and R_T is the total resistance estimated from the experimental spectrum at low frequency intercept of the semicircle with the real axis. Similarly, the bulk conductivity (σ_g) has been calculated using

bulk resistance (R_g) value obtained from fit data. It is also seen that the value of ΣR_i from fit data (Table 6) equals to the value of R_{Total} estimated from experimental spectrum (Table 7) which once again confirms the validity of the proposed equivalent circuits.

AC conductivity study

The frequency dependence of a.c. conductivity i.e. $\log\sigma$ vs $\log\omega$ plots for 4-methylpyridine-ICl complex is characterised by three distinct regimes (i) low frequency polarisation region (ii) the medium frequency plateau region and (iii) high frequency dispersion region (Fig. 6). But for pyridine-ICl and 3,5-dimethylpyridine-ICl complex, only the later two regions

Table 6 Fitted equivalent circuit parameters for the CT complexes

T (K)	R1(Ω^{-1})	C1(F)	R2(Ω^{-1})	C2(F)	R3(Ω^{-1})	C3(F)	$\Sigma R_i(\Omega^{-1}$)
Pyridine-ICl							
303	1.12×10^5	4.53×10^{-11}	9.63×10^5	2.60×10^{-11}	1.31×10^6	8.80×10^{-11}	2.38×10^6
313	9.51×10^4	3.67×10^{-11}	5.70×10^5	2.99×10^{-11}	2.79×10^5	1.90×10^{-10}	9.44×10^5
318	8.45×10^4	2.50×10^{-11}	3.85×10^5	2.50×10^{-11}	2.24×10^5	2.09×10^{-10}	6.94×10^5
323	8.31×10^4	2.28×10^{-11}	2.91×10^5	2.75×10^{-11}	1.23×10^5	3.24×10^{-10}	4.97×10^5
333	7.91×10^4	1.86×10^{-11}	1.00×10^5	5.05×10^{-11}	2.96×10^4	1.13×10^{-9}	2.09×10^5
343	5.90×10^4	1.67×10^{-11}	3.40×10^4	1.04×10^{-10}	6.37×10^3	3.79×10^{-9}	9.94×10^4
353	4.32×10^4	1.69×10^{-11}	1.04×10^4	3.10×10^{-10}	1.43×10^3	1.61×10^{-8}	5.50×10^4
3,5-dimethylpyridine-ICl							
303	7.72×10^4	3.65×10^{-11}	8.26×10^5	1.51×10^{-11}	4.14×10^5	1.72×10^{-10}	1.32×10^6
318	5.55×10^4	2.46×10^{-11}	3.72×10^5	1.61×10^{-11}	1.25×10^5	5.42×10^{-10}	5.53×10^5
323	3.47×10^4	6.92×10^{-12}	1.36×10^5	2.00×10^{-11}	3.82×10^4	1.16×10^{-9}	2.09×10^5
	CPE 1		R1(Ω^{-1})	CPE 2			
	Ca 1	Phi 1		Ca 2	Phi 2		
333	1.57×10^{-9}	6.43×10^{-1}	7.63×10^4	4.33×10^{-11}	4.25		7.63×10^4
338	1.60×10^{-9}	6.46×10^{-1}	5.09×10^4	6.04×10^{-11}	4.31		5.09×10^4
343	4.54×10^{-9}	5.78×10^{-1}	2.77×10^4	1.27×10^{-10}	4.28		2.77×10^4
4-methylpyridine-ICl							
303	6.71×10^{-9}	6.23×10^{-1}	6.42×10^3	1.43×10^{-4}	5.17×10^{-1}		6.42×10^3
313	5.38×10^{-9}	6.81×10^{-1}	4.38×10^3	2.50×10^{-4}	4.85×10^{-1}		4.38×10^3
323	4.99×10^{-7}	3.79×10^{-1}	1.57×10^3	5.93×10^{-4}	7.73×10^{-1}		1.57×10^3
333	2.34×10^{-6}	3.12×10^{-1}	7.99×10^2	5.71×10^{-4}	7.88×10^{-1}		7.99×10^2
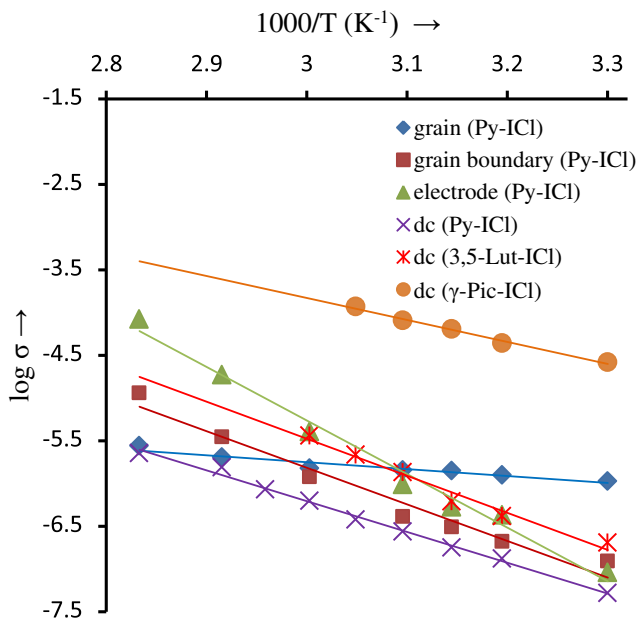
Fig. 5 Arrhenius plots of σg, σgb and σel for pyridine-ICl and σdc of the three complexes

a 4-methylpyridine-ICl

b 3,5-dimethylpyridine-ICl

c Pyridine-ICl

Fig. 6 Variation of a.c. conductivity with frequency for **a** 4-methylpyridine-ICl, **b** 3,5-dimethylpyridine-ICl and **c** pyridine-ICl complexes at various temperatures

are observed. In case of pyridine-ICl and 3,5-dimethylpyridine-ICl complex, the absence of the first low frequency regime attributed that there is no/negligible interfacial polarisation. In the low frequency region, conductivity increases with the increase in frequency which is attributed to the polarization at the electrode-sample interface. Here, flow of the charges accumulated at the interface is responsible for increase in conductivity. In the intermediate plateau region, conductivity is almost frequency independent and is equal to the bulk or d.c. conductivity of the sample. The higher frequency dispersion region can be explained by Jonscher's universal power law [43]
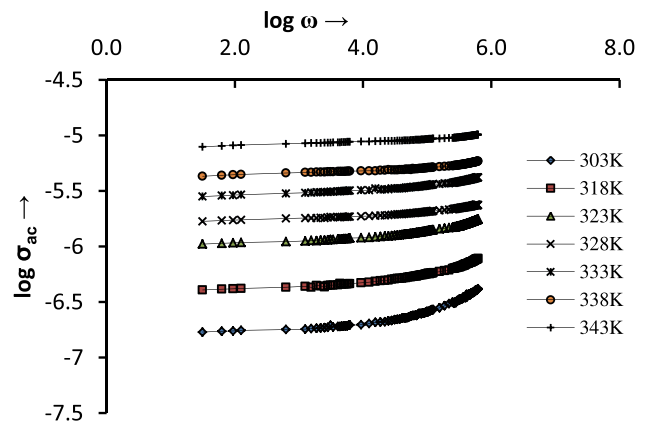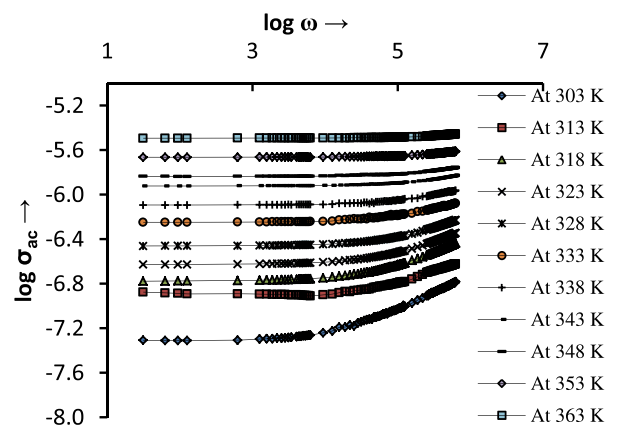
$$\sigma_{ac} = \sigma_{dc} + A\omega^s \qquad (6)$$

where σ_{ac} and σ_{dc} are the a.c. and d.c. conductivity, respectively, ω is the angular frequency which equals to $\omega = 2\pi f$, A is a constant and S is the frequency exponent having values between 0 and 1. From the slope of the plot between $\log\sigma$ versus $\log\omega$, the frequency exponent S can be obtained and the intercept of the horizontal portion on the vertical axis equals to $\log\sigma_{dc}$.

It is seen that as temperature increases, conductivity increases at all frequencies which attributes to thermal activation. It is also observed that the characteristic frequency, (the frequency at which dispersion region started to deviate from the d.c. conductivity plateau) at which relaxation effect begins to appear, shifted to the higher frequency with increase in temperature and arrived at a position beyond the measured frequency window limit. Another interesting observation is that the dispersion is more prominent at lower temperature, which is reflected in the value of S which decreases with the rise of temperature as shown in Fig. 7. All these observations
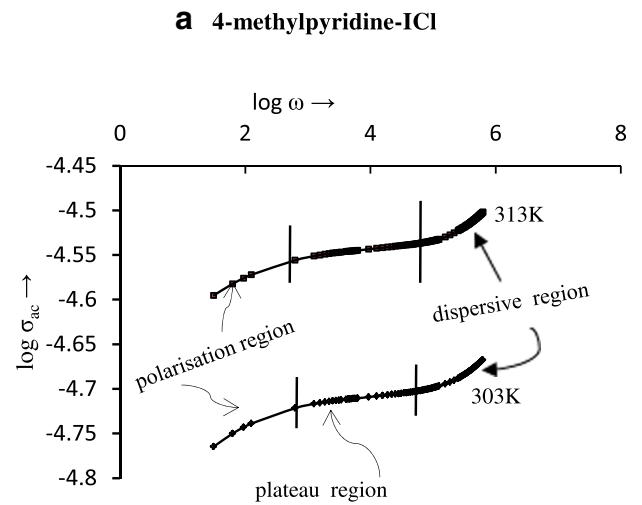
indicate that the tested materials exhibit semiconducting behaviour and the a.c. conduction mechanism is due to barrier hopping [44, 45].

Table 7 Total conductivity and d.c. conductivity of the complexes at various temperatures

T (K)	$R_{total}(\Omega^{-1})$ (from Nyquist semicircle)	$\sigma_T = \frac{1}{R_{total}} \times \frac{t}{A}$ (Ω^{-1} cm^{-1})	$\sigma_{dc}(\Omega^{-1}$ cm$^{-1})$ (from intercept of the linear portion of $\log\sigma_{ac}$ vs $\log\omega$ plot by LCR meter)	$\sigma_{dc}(\Omega^{-1}$ cm$^{-1})$ (from the slope of the I/V plots by source meter)
Pyridine-ICl 303	2.41×10^6	4.95×10^{-8}	5.01×10^{-8}	5.20×10^{-8}
313	9.50×10^5	1.25×10^{-7}	1.28×10^{-7}	1.32×10^{-7}
318	7.14×10^5	1.67×10^{-7}	1.69×10^{-7}	1.77×10^{-7}
323	5.05×10^5	2.36×10^{-7}	2.38×10^{-7}	2.74×10^{-7}
328	–	–	3.48×10^{-7}	3.76×10^{-7}
333	2.11×10^5	5.64×10^{-7}	5.66×10^{-7}	6.25×10^{-7}
338	–	–	8.09×10^{-7}	8.50×10^{-7}
343	9.97×10^4	1.19×10^{-6}	1.19×10^{-6}	1.54×10^{-6}
353	5.50×10^4	2.16×10^{-6}	2.17×10^{-6}	2.26×10^{-6}
3,5-dimethylpyridine-ICl				
303	1.36×10^6	1.76×10^{-7}	1.80×10^{-7}	2.03×10^{-7}
318	5.59×10^5	4.29×10^{-7}	4.30×10^{-7}	4.14×10^{-7}
323	2.11×10^5	1.14×10^{-6}	1.11×10^{-6}	1.35×10^{-6}
328	1.33×10^5	1.80×10^{-6}	1.79×10^{-6}	2.16×10^{-6}
333	7.74×10^4	3.09×10^{-6}	3.01×10^{-6}	3.63×10^{-6}
4-methylpyridine-ICl				
303	6.37×10^3	1.97×10^{-5}	1.95×10^{-5}	2.62×10^{-5}
313	4.36×10^3	2.87×10^{-5}	2.86×10^{-5}	4.37×10^{-5}
318	2.21×10^3	5.67×10^{-5}	5.59×10^{-5}	6.41×10^{-5}
323	1.54×10^3	8.13×10^{-5}	7.99×10^{-5}	8.07×10^{-5}
328	1.06×10^3	1.18×10^{-4}	1.19×10^{-4}	1.17×10^{-4}

Measurement of ionic transport number

From the current vs time plots (Fig. 8) at room temperature, the total ionic transport number (t_{ion}) of the complexes were
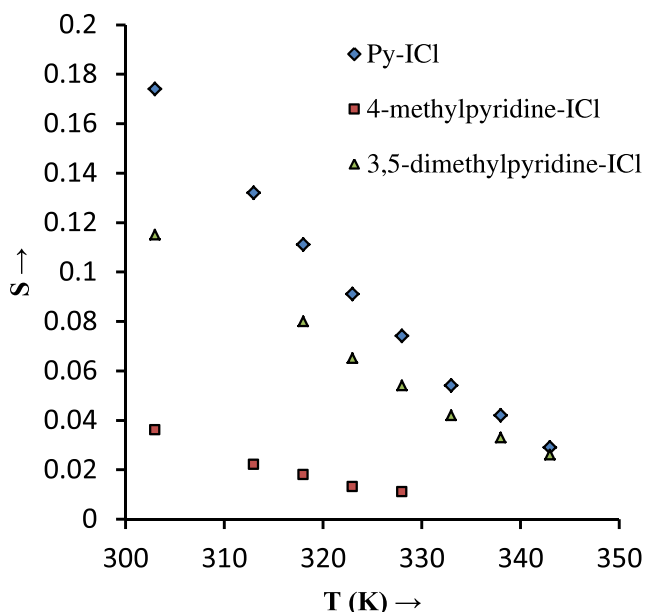
Fig. 7 Variation of frequency exponent(s) with temperature

calculated using the Eq. 1. The values of t_{ion} (Table 2) imply that the conduction mechanism in pyridine-ICl complex (t_{ion} = 0.11) is predominantly electronic, in 3,5-dimethyl-ICl complex (t_{ion} = 0.58) is mixed ionic-electronic and in 4-methylpyridine-ICl complex (t_{ion} = 0.95) is mainly ionic as came across from impedance spectra.

DC conductivity measurement

The current-voltage characteristics of the samples in the pellet form recorded at various temperatures by using Keithley 2400 source meter are shown in Fig. 9 (S6a, b). It is observed that the I/V curves are linear indicating the ohmic behaviour. From the slope of the I/V curve d.c. conductivity can be calculated by using the following relation

$$\sigma_{dc} = slope \times \frac{t}{A} \qquad (7)$$

where t is the thickness and A is the surface area of the sample. The d.c. conductivities measured from the I/V curves (using source meter) are well agreement to those calculated from the intercept of $\log\sigma$ versus $\log\omega$ plot (Table 7). Further, total conductivity, σ_{Total}, measured from the experimental Nyquist

Fig. 8 Current vs time plots of **a** pyridine-ICl, **b** 3,5-dimethylpyridine-ICl and **c** 4-methylpyridine-ICl complex at 303 K
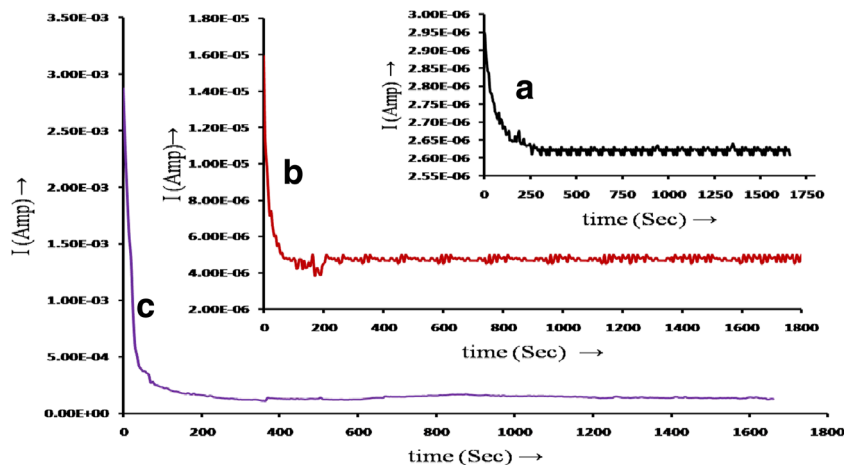
plots nearly equals to the σ_{dc} values and follows the Arrhenius law (Fig. 5). The activation energy for d.c. conductivity, calculated from the Arrhenius plots are 0.51, 0.71 and 0.86 eV for 4-methylpyridine-ICl, pyridine-ICl and 3,5-dimethylpyridine-ICl, respetively.

The increasing order of conductivity at any particular temperature is pyridine-ICl < 3,5-dimethylpyridine-ICl << 4-methylpyridine-ICl. Among the three, the highest conductivity of 4-methylpyridine-ICl complex is due to the higher ionisation (t_{ion} = 0.95) and lower band gap (E_g = 2.21 eV); on the contrary, pyridine-ICl complex with lower ionisation (t_{ion} = 0.11) and higher band gap (E_g = 2.85 eV) reveals lowest conductivity.

Conclusion

The investigations of the three charge transfer complexes by complex impedance spectra and ionic transport number measurements confirm that 4-methylpyridine-ICl can be considered purely ionic which originates from (γ-Pic$_2$-I)$^+$ and ICl$_2^-$ ions, while 3,5-dimethylpyridine-ICl is a mixed ionic-electronic conductor and pyridine-ICl is predominantly electronic in nature. The electrical properties of pyridine-ICl and 4-methylpyridine-ICl can be described by equivalent circuits –(RC)–(RC)–(RC)– and –(Rcpe)–(cpe)– respectively. The former circuit corresponds to grain, grain boundary and electrode contributions whereas the latter circuit corresponds to bulk resistance and double layer capacitance of electrode-material interface. Interestingly, electrical properties of 3,5-dimethylpyridine-ICl complex fits in both the equivalent circuits. At low temperature, it corresponds to that of –(RC)–(RC)–(RC)– and at high temperature it corresponds to –(Rcpe)–(cpe)–. The nature of the variation of d.c. conductivity with temperature suggests semiconducting behaviour with activation energy 0.71, 0.51 and 0.86 eV for pyridine-ICl, 4-methylpyridine-ICl and 3,5-dimethylpyridine-ICl complexes, respectively. The frequency dependence of a.c. conductivity obeys the Jonscher's power law.

Fig. 9 Current-voltage plots of 3,5-dimethylpyridine-ICl complex at different temperatures
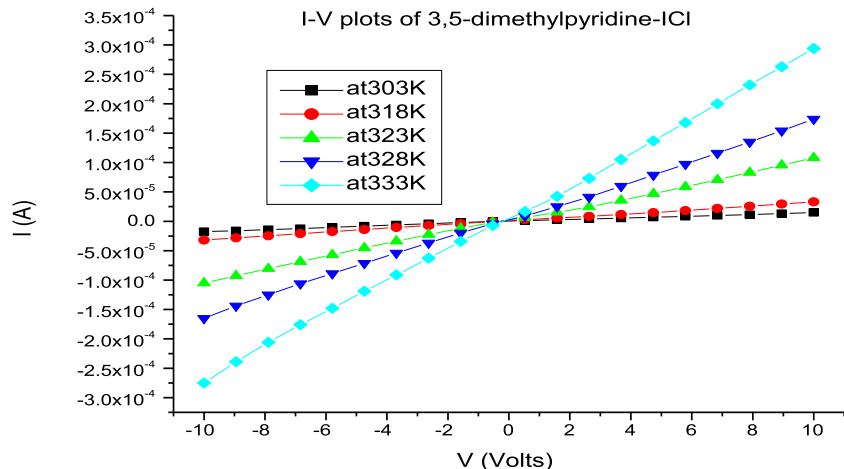
References

1. Mulliken RS (1950) Structures of complexes formed by halogen molecules with aromatic and with oxygenated solvents. J Am Chem Soc 72:600–608
2. Mulliken RS (1952) Molecular compounds and their spectra II. J Am Chem Soc 74:811–824
3. Mori H (2008) Introduction of organic superconducting materials. In: Sun SS, Dalton LR (eds) Introduction to organic electronic and optoelectronic materials and devices. CRC, New York, pp. 263–286
4. Okamoto H, Mitani T, Tokura Y, Koshihara S, Komatsu T, Iwasa Y, Koda T, Saito G (1991) Anomalous dielectric response in tetrathiafulvalene-p-chloranil as observed in temperature- and pressure-induced neutral-to-ionic phase transition. Phys Rev B 43: 8224–8232
5. John Ferraris DO, Cowan V, Jr W, Perlstein JH (1973) Electron transfer in a new highly conducting donor-acceptor complex. J Am Chem Soc 95:948–949. doi:10.1021/ja00784a066
6. Coleman LB et al. (1973) Superconducting fluctuations and the peierls instability in an organic solid. Sol State Commun 12: 1125–1132
7. Jurchescu OD, Goetz KP, et al. (2014) Charge-transfer complexes: new perspectives on an old class of compounds. J Mater Chem C 2: 3065–3076. doi:10.1039/c3tc32062f
8. Gutmann F, Lyons LE (1967) Organic semiconductors. John Wiley and Sons Inc., New York
9. Ashwell GJ (ed) (1992) Molecular electronics. Research Studies Press, Taunton
10. Akamatu H, Inokuchi H, Matsunaga Y (1954) Electrical conductivity of the perylene-bromine complex. Nature 173:168–169
11. Akamatu H, Inokuchi H, Matsunaga Y (1956) Organic semiconductors with high conductivity. I. Complexes between polycyclic aromatic hydrocarbons and halogens. Bull Chem Soc Jpn 29:213–218
12. Nisizaki S, Kusakawa H (1963) The electrical conduction of the p-Phenylenediamine iodine complex. Bull Chem Soc Jpn 36: 1681–1683
13. Singh RA, Singh VK (1997) Mixed conduction in charge transfer materials based on aromatic diamines and iodine having different mole ratios. Bull Mater Sci 20(3):305–315
14. Mulliken RS, Person WB (1969) Molecular complexes—a lecture and reprint volume. Wiley, New York
15. Foster R (1969) Organic charge transfer complexes. Academic Press, London
16. Gur'yanova EN, Gol'dshtein IP, Romm IP (1975) Donor-acceptor bond. Keter Publishing House, Jerusalem
17. Akutagawa T, Uchigata M, Hasegawa T, Nakamura T, Nielsen KA, Jeppesen JO, Brimert T, Becher J (2003) Langmuir-Blodgett films of charge-transfer complexes between an Amphiphilic Monopyrrolo-TTF and TCNQ derivatives. J Phys Chem B 107:13929–13938
18. Carlin RL (1985) Magnetochemistry. Springer-Verlag, New York
19. Kahn O (1993) Molecular magnetism. VCH, Weinheim
20. Saito G (2008) Murata T (2008) Mixed valency in organic charge transfer complexes. Phil Trans R Soc A 366:139–150. doi:10.1098/rsta.2007.2146
21. Macdonald JR (1987) Impedance spectroscopy. Wiley, New York
22. Macdonald JR (1987) Impedance spectroscopy: emphasizing solid materials and systems. Wiley, New York
23. Barsoukov E, Macdonald JR (2005) Impedance sprectroscopy: theory, experiment, and applications, 2nd edn. Wiley-Interscience, New York
24. MEISP, March, 2002.Korea: Kumho Chemical Laboratories
25. Huggins RA (2002) Simple method to determine electronic and ionic components of the conductivity in mixed conductors a review. Ionics 8:300–313
26. Gogoi A, Sarma SN (2015) Conductivity study of poly(acrylonitrile-co-2-vinylpyridine) complexed with vinyl acetic acid and 4-pentenoic acid. Ionics 22(1):77–84. doi:10.1007/s11581-015-1529-5
27. Goswami S, Dutta A (2011) Measurement of ionic conductivity of poly (N-vinylimidazole) and its fluoroborate salt in solid state. Ionics 17(7):627–632. doi:10.1007/s11581-011-0554-2
28. Gabes W, Stufkens DJ (1973) Electronic absorption spectra of symmetrical and asymmetrical trihalide ions. Spectrochemica Acta 30A:1835–1841
29. Tauc J, Grigorovici R, Vancu A (1966) Optical properties and electronic structure of amorphous germanium. Phys Status Sol 15: 627–637
30. Vennila P, Govindaraju M, Venkatesh G (2013) Scaled quantum chemical studies of the structure, vibrational spectra, force constants and first-order Hyperpolarizability of 3,5-dimethylpyridine. Elixir Vib Spec 65B:20204–20211
31. Marcos JI, Oter JC, Tocon IL, Arenas JF (1999) Vibrational spectra of methylpyridines. J Mol Struct 476:139–150
32. Akyiiz S, Dempster AB, Morehouse RL, Suzuki S (1973) An infrared and Raman spectroscopic study of some metal pyridine tetracyanonickelate complexes. J Mol Struct 17(1):105–125. doi:10.1016/00222860(73)850471
33. Kantarci Z, Bayrak C, Bayari S (1997) An infrared and Raman spectroscopic study on the Hofmann-td-type complexes: $ML_2M'(CN)_4$, M = Mn or Zn, M' = Zn, Cd or Hg, L = pyridine, α-, β- or γ-picoline. J Mol Struct 407:155–163
34. Akyuz S, Pasaoglu H, Davies JED (1994) A vibrational spectroscopic study of Hofmann type complexes of 3- and 4-methylpyridines. J Mol Struct 317(3):215–221
35. Person WB, Humphrey RE, Deskin WA, Popov AI (1958) Infrared spectra of iodine monochloride charge-transfer complexes. J Am Chem Soc 80:2049–2053
36. Ginn SGW, Haque I, Wood JL (1968) The vibration spectra of the complexes pyridine—bromine, and pyridine—bromine chloride. Spectrochim Acta A: Mol Spectrosc 24(10):1531–1542
37. Katcka M, Urbanski T (1968) NMR spectra of pyridine, picolines and hydrochlorides and of their hydrochlorides and methiodides. Bulletin de L'academie Polonaise des Sciences XVI(7):347–350
38. Romming C (1972) Refinement of the crystal structure of charge transfer compound pyridine-iodomonochloride. Acta Chem Scand 26:1555–1560
39. Alexaner L, Klug HP (1950) Determination of crystallite size with the X-ray spectrometer. J Appl Phys 21:137–142. doi:10.1063/1.1699612
40. Hafidi E, Omari ME, Omari ME, Bentayeb A, Bennazha J, Maadi AE, Chehbouni M (2013) Arab J Chem 6:253–263. doi:10.1016/j.arabjc.2011.01.028
41. Bauerle JE (1969) Study of solid electrolyte polarization by a complex admittance method. J Phys Chem Solids 30:2657–2670
42. Yang X, Tan S, Liang T, Wei B, Wu Y (2016) Synthesis, characterization, and electrochemical properties of smectic pyridinium salts with inorganic dihydrogen phosphate ions. Ionics 22(1):85–92. doi:10.1007/s11581-015-1524-x
43. Jonscher AK (1977) The 'universal' dielectric response. Nature 267:673–679. doi:10.1038/267673a0
44. Elliott SR (1977) A theory of a.c. conduction in chalcogenide glasses. Philos Mag 36:1291–1304. doi:10.1080/14786437708238517
45. Ali AA, Shaaban MH (2010) Electrical properties of LiBBaTe glass doped with Nd_2O_3. Solid State Sci 12:2148–2154. doi:10.1016/j.solidstatesciences.2010.09.016